NANO LETTERS

pubs.acs.org/NanoLett

Using the Angle-Dependent Resonances of Molded Plasmonic Crystals To Improve the Sensitivities of Biosensors

Hanwei Gao,[§,†] Jiun-Chan Yang,[§,†] Julia Y. Lin,[†] Andreea D. Stuparu,[||] Min Hyung Lee,[†] Milan Mrksich,[||] and Teri W. Odom*[,†,‡]

[†]Department of Chemistry, [‡]Department of Materials Science and Engineering, Northwestern University, Evanston, Illinois 60208, and [||]Department of Chemistry, University of Chicago, Chicago, Illinois 60637

ABSTRACT This paper describes how angle-dependent resonances from molded plasmonic crystals can be used to improve real-time biosensing. First, an inexpensive and massively parallel approach to create single-use, two-dimensional metal nanopyramidal gratings was developed. Second, although constant in bulk dielectric environments, the sensitivities (resonance wavelength shift and resonance width) of plasmonic crystals to adsorbed molecular layers of varying thickness were found to depend on incident excitation angle. Third, protein binding at dilute concentrations of protein was carried out at an angle that optimized the signal to noise of our plasmonic sensing platform. This angle-dependent sensitivity, which is intrinsic to grating-based sensors, is a critical parameter that can assist in maximizing signal to noise.

KEYWORDS Biosensing, plasmonic crystal, molding, protein binding, sensitivity

Surface plasmon resonance (SPR)-based sensing is a label-free, real-time analytical technique that has greatly impacted medical diagnostics,[1,2] environmental monitoring,[3,4] and food safety.[5,6] Without using fluorescent or enzymatic labels that can perturb molecular interactions, plasmonic sensors enable more accurate measurements of binding kinetics at low analyte concentrations.[7] Most SPR sensors rely on the Kretschmann configuration;[8] however, the prism optics inhibit high-throughput image sensing for screening applications. This problem can be overcome using grating-based sensors[9−13] because surface plasmon resonances can be generated using broad band, free-space illumination instead of total internal reflection at a single wavelength via prism excitation. Furthermore, grating elements can be made as small as a few micrometers,[14,15] which is promising for the production of compact, multiplexed sensing chips.

Compared with most prism-based devices, grating-based sensors exhibit low sensitivity,[7,16] which is a major disadvantage. Efforts to improve sensitivities have focused on engineering the topography and materials of the gratings;[17,18] however, these processes typically involve serial patterning using focused ion beam milling[19] or electron beam lithography,[20] which increases the fabrication costs and limits the throughput. Here we describe an inexpensive and simple sensing platform based on molded and disposable plasmonic crystals that support bulk refractive index sensitivities as well as protein binding kinetics comparable to those of commercial SPR sensors. Moreover, we found that the sensing response (wavelength shift and resonance width) of gold nanopyramidal gratings to adsorbed polyelectrolyte layers of different thicknesses depended strongly on the excitation angle of incident light. Taking advantage of these angle-dependent resonances to improve signal to noise, we performed the sensitive measurement of protein binding using a plasmonic crystal sensor.

Figure 1A summarizes the nanofabrication procedure to prepare molded plasmonic crystals. First, a Si template (master) of a 2D square array of nanopyramidal pits was generated using soft interference lithography followed by PEEL.[21,22] The nanopyramidal gratings had a lattice constant $a_0 = 400$ nm, and the unit cells had edge lengths = 300 nm. Next, high-quality replicas of the Si template were formed by first creating a composite poly(dimethylsiloxane) (PDMS) mold[23] with inverted topographical features and then molding UV-curable polyurethane (PU) against this patterned PDMS (Figure 1B). Hundreds of PU replicas can be generated from a single PDMS mold. Finally, 150 nm of gold was deposited by e-beam onto the molded PU substrates with nanopyramidal unit cells supported on glass slides to produce 2D plasmonic crystals (Figure 1C).

Our nanofabrication procedure can create large-area (>1 cm^2) plasmonic sensing substrates with high uniformity (Figure 2A). We characterized their sensing response using a home-built rotational stage capable of real-time measurements (Figure 2B). Angle-dependent reflection spectra were measured under collimated, p-polarized white light illumination ($\lambda = 400-1000$ nm). Although the angles of incident light θ and reflected light could be varied independently, we

* To whom correspondence should be addressed, todom@northwestern.edu.

§ These authors contributed equally to this work.

Received for review: 04/2/2010
Published on Web: 05/28/2010

DOI: 10.1021/nl101165r | *Nano Lett.* **2010,** *10,* 2549–2554

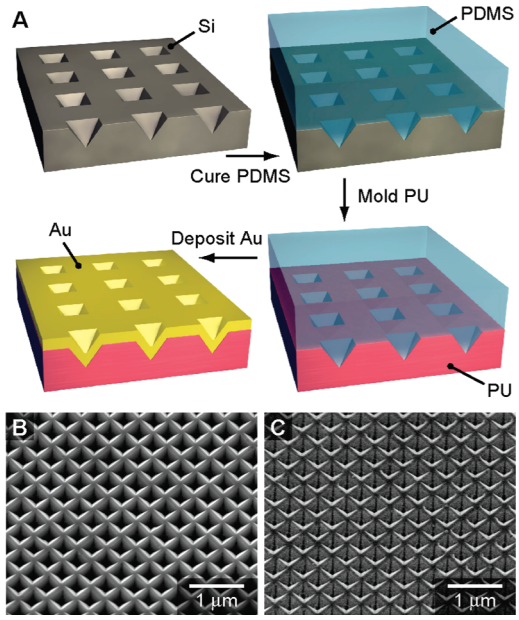

FIGURE 1. Bench-top fabrication of molded plasmonic crystals. (A) Scheme to generate low-cost plasmonic gratings using nanopyramidal polyurethane (PU) replicas of a Si template followed by electron-beam deposition of gold. Scanning electron microscopy (SEM) images of (B) Si template and (C) gold-coated PU replica showing high uniformity and fidelity.

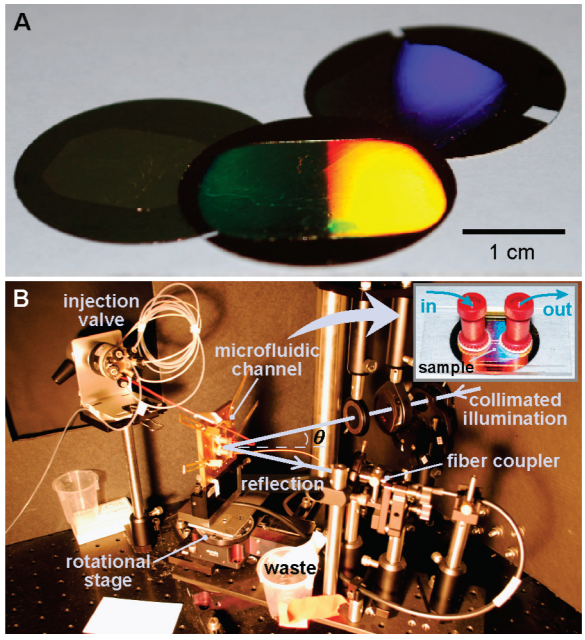

FIGURE 2. Optical photographs of sensing substrates and experimental setup. (A) PU-molded plasmonic crystals on glass coverslips coated with 150 nm of gold. Patterned areas were >1 cm^2. (B) Real-time sensing and angle-resolved spectroscopy setup with a microfluidic cell mounted on a home-built rotational stage.

focused only on the zero-order reflection spectra. By monitoring the most intense plasmon resonance (typically the (−1,0) surface plasmon polariton (SPP) mode[24]) and using a Lorentzian fit,[7] we could detect small changes in wavelength ($\Delta\lambda \sim 3.6 \times 10^{-4}$ nm) as analytes bound to the plasmonic crystal surface. A microfluidic channel system was overlaid on the plasmonic substrate to measure protein binding kinetics without mass-transfer limitations (Figure 2B, inset and Methods).

Figure 3A shows that the SPP resonances from the molded plasmonic crystals in air ($n = 1.00$) were observed as minima in the reflection spectra. Similar to our previous results on plasmonic crystals based on etched Si substrates,[25] as the excitation angle θ increased, the (−1,0) SPP mode shifted to longer wavelengths, and the full width at half-maximum (fwhm) of the resonance narrowed dramatically. To compare the sensitivities of molded plasmonic crystals to state-of-the-art SPR sensors,[7] we focused on the narrow resonance obtained at $\theta = 60°$ (fwhm = 9.15 nm). We selected this high angle for comparison because the wavelength shift $\Delta\lambda$ under different bulk dielectric environments is *independent* of θ; thus, only the narrowest resonance is needed to achieve the highest figure of merit (FOM $= \Delta\lambda$/fwhm).[24] Calibrating the plasmonic substrates using NaCl solutions of different concentrations (Methods), we determined the refractive index resolution to be 9.7×10^{-7} RIU (refractive index unit) with a temporal resolution of 2 s, which is very similar to the plasmon-based sensors that are currently available. However, this *bulk* refractive index sensitivity represents neither the appropriate environment nor necessary conditions for biosensing because analytes are detected at a distance much closer to the surface (several nanometers) than the extent of the evanescent SPP fields (hundreds of nanometers).

In order to determine the *surface* sensitivity, which will be important for biosensing, we used layer-by-layer assembly to organize N polyelectrolyte bilayers of known thickness and refractive index on molded gold plasmonic crystals. Each bilayer was composed of a poly(dimethyldiallylammonium chloride) (PDDA) layer and duplex DNA layer (Methods) for a bilayer thickness of ca. 6 nm.[26] Figure 3B shows how the (−1,0) SPP mode red-shifted by an amount $\Delta\lambda$ as N increased. Significantly, the slopes of the $\Delta\lambda$ vs N relation *decreased* at higher θ, which was different from the slopes of the $\Delta\lambda$ vs refractive index n relation for bulk sensitivities, which were the same for all θ.[24] Thus for molecular sensing, selection of the conditions to optimize the figure of merit is not straightforward because both $\Delta\lambda$ and fwhm depend on the excitation angle θ.

To understand this angle-dependent (or surface) sensitivity, we need to consider the evanescent nature of the SPP electromagnetic fields. The decay length Z_d (where the amplitude drops to $1/e$) is determined primarily by the resonance wavelength λ[27]

$$Z_d = \mathrm{Im}\left[\frac{\lambda}{2\pi}\left(\frac{\varepsilon_d + \varepsilon_{Au}}{\varepsilon_d^{\,2}}\right)^{1/2}\right] \quad (1)$$

DOI: 10.1021/nl101165r | *Nano Lett.* **2010,** *10,* 2549–2554

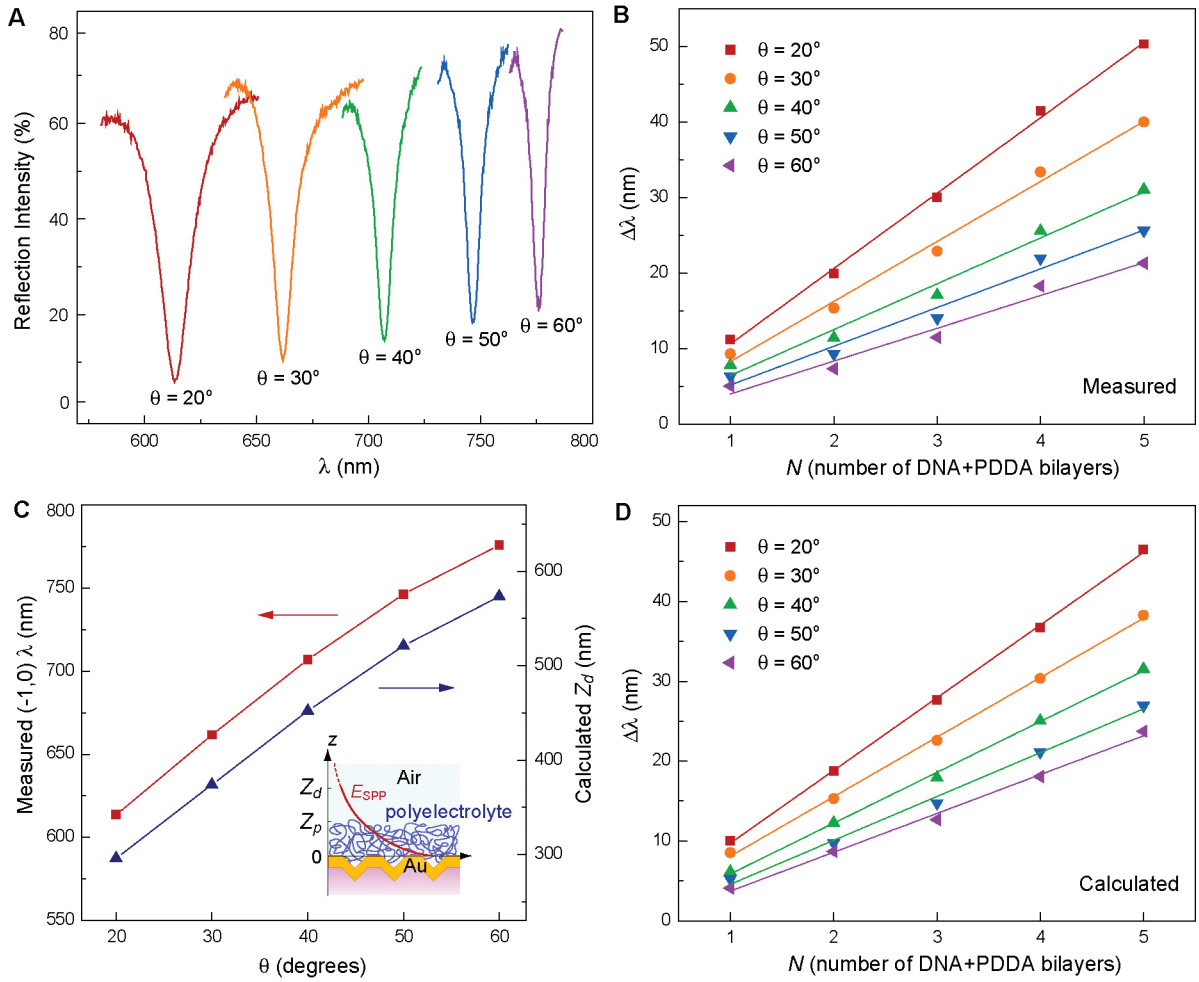

FIGURE 3. Demonstration of angle-dependent sensitivities from molded plasmonic crystals using polyelectrolyte multilayers. (A) Narrow and intense (−1,0) SPP resonances were observed in gold plasmonic crystals in air. As θ increased, the resonance shifted to longer wavelength, and the fwhm decreased. (B) The (−1,0) resonance red-shifted as the number of layers N increased. The amount of shift $\Delta\lambda$ is larger at lower θ. (C) The measured resonant wavelength λ and the calculated decay length Z_d of the (−1,0) SPP mode increased at larger θ. (D) Calculated angle-dependent $\Delta\lambda$−N relations, which agree quantitatively with the measured results in (B).

where ε_{Au} and ε_d are the relative permittivities of gold[28] and the adjacent dielectric material. As θ increases, the (−1,0) SPP resonance of the plasmonic crystal red shifts, and Z_d also increases (Figure 3C). Hence, at higher θ, the ratio (Z_p/Z_d) of the analyte thickness $Z_p = (d_{PDDA} + d_{DNA})N$ to the decay length of the SPP evanescent field Z_d decreases (Figure 3C, inset), resulting in a smaller $\Delta\lambda$. The relationship between $\Delta\lambda$ and N can be numerically calculated by solving the characteristic equation[29]

$$Z_p \frac{2\pi}{\lambda}(\varepsilon_{eff} - \varepsilon_{SPP})^{1/2} - \arctan\left[\frac{\varepsilon_{eff}}{\varepsilon_d}\left(\frac{\varepsilon_{SPP} - \varepsilon_d}{\varepsilon_{eff} - \varepsilon_{SPP}}\right)^{1/2}\right] - \arctan\left[\frac{\varepsilon_{eff}}{\varepsilon_m}\left(\frac{\varepsilon_{SPP} - \varepsilon_m}{\varepsilon_{eff} - \varepsilon_{SPP}}\right)^{1/2}\right] = 0 \quad (2)$$

and using an effective media approximation for the polyelectrolyte layer, where

$$\varepsilon_{eff} = n_{eff}^2 = \left(\frac{n_{PDDA}d_{PDDA} + n_{DNA}d_{DNA}}{d_{PDDA} + d_{DNA}}\right)^2 \quad (3)$$

ε_{SPP} is the effective index of the SPP modes.[30] n_{eff} was calculated to be 1.47 using values from ref 26 for the thicknesses (d_{PDDA} and d_{DNA}) and refractive indices (n_{PDDA} and n_{DNA}) of the polyelectrolyte layers. Although the $\Delta\lambda$−N relation is nonlinear at large N (Figure S1 in Supporting Information), the resonance shifts linearly with N for small thicknesses of the polyelectrolyte ($N < 5$) (Figure 3B,D). Quantitative agreement between the experimental and theoretical $\Delta\lambda$−N (Table S1 in Supporting Information) verified that $\Delta\lambda$ depended on Z_p/Z_d. Specifically, by reducing θ, we could generate SPP fields with smaller decay lengths, which resulted in a greater $\Delta\lambda$.

The angle-dependent sensitivity of molded plasmonic crystals can be used to optimize signal to noise for real-time biomolecular sensing. As a model system to perform

DOI: 10.1021/nl101165r | Nano Lett. 2010, 10, 2549–2554

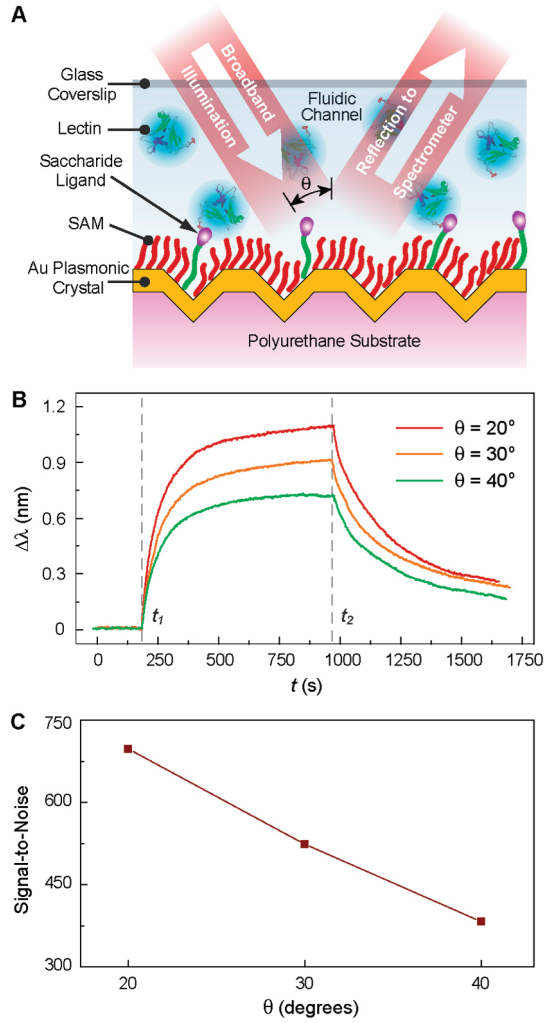

FIGURE 4. Optimizing signal-to-noise for real-time biosensing. (A) Scheme depicting the side view of a microfluidic channel for measuring lectin binding to disaccharide immobilized on a gold plasmonic crystal. (B) Sensorgrams obtained under different θ showed angle-dependent sensitivity in real-time detection. (C) Dependence of signal to noise on θ for lectin−disaccharide binding. For this assay, lower θ was best to optimize signal to noise.

the sensitive measurement of protein binding at dilute concentrations (5 μM) of protein, we used the binding of *Arachis hypogaea* lectin to the disaccharide Galβ(1, 3)GalNAc immobilized to a monolayer (Figure 4A). The binding affinity for this interaction is approximately 5 μM,[31] which allows both the dissociation and association kinetics to be determined within a reasonable time scale (minutes). The sensing surface was prepared by first functionalizing the molded gold plasmonic crystal with a self-assembled monolayer presenting maleimide and tri(ethylene glycol) groups.[32] The monolayer was then treated with a thiol-terminated disaccharide to allow immobilization of the ligand to the maleimide group. The maleimide groups, and therefore the disaccharides, were presented at a 5% density within the mixed monolayer.

TABLE 1. Kinetic Constants of Lectin−Sugar Binding Measured at Different θ

	k_a (M^{-1} s^{-1})	k_d (s^{-1})
$\theta = 20°$	1802	2.54×10^{-3}
$\theta = 30°$	1813	2.43×10^{-3}
$\theta = 40°$	1814	2.70×10^{-3}
prism based[a]	1720	1.73×10^{-3}

[a] Rates measured using a BIAcore 2000 SPR system on a planar gold substrate.

This surface coverage optimizes the density of ligand without introducing crowding (and loss of activity) of the ligands and without compromising the protein resistance of the ethylene glycol groups. To verify the presence of the alkanethiolates in the monolayer and the immobilization of the disaccharide, we used self-assembled monolayer matrix assisted laser desorption ionization time-of-flight mass spectrometry (SAMDI-MS) (Figure S3 in Supporting Information).[33,34]

Sensorgrams were obtained by monitoring changes in the (−1,0) SPP resonance wavelength with a resolution of 2 s (Figure 4B). A 5 μM lectin solution was injected with a constant flow rate of 60 μL/min between time points t_1 and t_2; abrupt changes after lectin injection and buffer washing were observed in the sensing curves. Consistent with the surface characteristics of the polyelectrolyte layers (larger $\Delta\lambda$ at smaller θ) in Figure 3B, angle-dependent sensitivity was observed at every time point. Note that the kinetic constants determined at different θ were similar and also in agreement with measurements from a commercial prism-based sensor (Table 1). The association rates k_a and dissociation rates k_d between the lectin protein and the disaccharide ligand were determined by the Langmuir model.[35] Although a narrower resonance could be obtained at larger θ (Figure S4 in Supporting Information), the wavelength shift $\Delta\lambda$ was smaller; both are critical to the signal-to-noise ratio ($S/N = \Delta\lambda_{max}$ /noise) (Figure 4C). Hence there is a trade-off between monitoring the narrowest resonance and the largest wavelength shift in real-time sensing. For a 5 μM lectin solution, we found that $\theta = 20°$ resulted in the maximum signal to-noise in our system (=1.1027 nm/1.5×10^{-3} nm = 698).

In conclusion, we demonstrated that plasmonic crystals with subwavelength features can be replicated with high fidelity and low cost using a simple molding method. The molded plasmonic substrates can produce bulk refractive index sensitivities comparable to prism-based SPR sensors and, in addition, measure protein binding at dilute concentrations. The angle-dependent surface sensitivity exhibited by nanopyramidal plasmonic crystals also applies to other gratings used for sensing; thus, the ability to tune the excitation angle provides a general approach to increase the signal-to-noise ratio in real-time measurements. Furthermore, molded plasmonic crystals produced protein binding constants similar to those from commercial SPR sensors. These disposable substrates can

DOI: 10.1021/nl101165r | *Nano Lett.* **2010,** *10,* 2549–2554

therefore be used for multiplexed kinetic studies and for point-of-care diagnostics.

Methods. ***Determination of Bulk Refractive Index Sensitivity and Noise Levels.*** Bulk index sensitivity was calibrated using 0.5, 4.0, and 10.0 wt % NaCl solutions in deionized water. The refractive indexes of the NaCl solutions were 1.3339, 1.3400, and 1.3505, respectively (Mettler Toledo http://us.mt.com). A bulk index sensitivity of 375 nm/RIU was obtained. To determine the refractive index (RI) resolution, the noise level was measured at a static RI point and represents twice the standard deviation of the monitored signal (i.e., at the resonance wavelength). The response signal from surfaces functionalized with molecules fluctuated more than the signal from unfunctionalized sensing substrates. Thus noise determined for molecular sensing (1.5×10^{-3} nm) was higher than that found in bulk index sensing (3.6×10^{-4} nm).

Assembly of Polyelectrolyte Bilayers. The gold sensing substrate was first incubated in a freshly prepared 2 mM ethanolic solution of carboxyl-terminated thiol ($HS-(CH_2)_{11}-COOH$, Sigma-Aldrich) for 16 h to form an ordered monolayer. The substrate was subsequently immersed in phosphate buffered saline (PBS, pH = 7.0) with poly(ethylenimine) (PEI, 1 mg/mL) (MW = 60 kDa, Sigma-Aldrich) to form a positively charged layer. After being rinsed with PBS buffer, the substrate was immersed in a solution of DNA (0.2 mg/mL, sodium salt from calf thymus, Sigma-Aldrich) and then in a solution of PDDA (0.5 mg/mL, MW = 400−500 kDa, Sigma-Aldrich) to form a polyelectrolyte bilayer. Multilayers were assembled in this layer-by-layer (LBL) fashion with PBS rinsing before the adsorption of the next layer. Conformal LBL assembly of the polyelectrolyte bilayers was confirmed using UV−vis absorption spectra (Figure S2 in Supporting Information).

Functionalization of the Sensing Substrates for Lectin Detection. Gold plasmonic crystals were immersed in an ethanolic mixture of 5% maleimide-terminated and tri(ethylene glycol)-terminated disulfide. The mixed monolayer was allowed to self-assemble overnight in the dark at 4 °C. Following monolayer formation, the grating was rinsed with PBS and dried under a stream of nitrogen gas. The substrate was subsequently soaked in a 0.1 mM solution of thiol-terminated dissacharide Galβ(1, 3)GalNAc dissolved in PBS (pH > 7) at room temperature for 3 h. After the immobilization of the sugar was complete, the substrate was washed again with PBS and dried under nitrogen before use in real-time sensing experiments, where lectin (5 μM) from *Arachis hypogaea* (peanut) was flowed over the surface.

Microfluidic System. The microfluidic channel consisted of a single slit (1 mm wide, 10 mm long) in a 250 μm silicone membrane (Grace Bio-Laboratories) sandwiched between the gold plasmonic crystal sensing substrate and a glass slide. The volume of the channel was 25 μL. Inlet and outlet holes were drilled through the glass slide to connect the tubing. A syringe pump (kdScientific) with an injection valve (Rheodyne 9725) was used to inject sample solutions with a constant flow rate of 60 μL/min.

Acknowledgment. This work was supported by the National Science Foundation under NSF Award Number CMMI-0826219, the Nanoscale Science and Engineering initiative under NSF Award Number EEC-0647560, and the Center of Cancer Nanotechnology Excellence at Northwestern University. This work used the NUANCE Center facilities, which are supported by NSF-MRSEC, NSF-NSEC, and the Keck Foundation. The authors thank Lan Ban for preparing the disaccharide reagent.

Supporting Information Available. Nonlinear relationship between the resonance shift and the polyelectrolyte thickness, UV−vis absorption spectrum of the LBL assembly, SAMDI mass spectra of surface functionalization for lectin−sugar binding, and the (−1,0) SPP resonances of gold plasmonic crystals on PU substrates in water. This material is available free of charge via the Internet at http://pubs.acs.org.

REFERENCES AND NOTES

(1) Cherif, B.; Roget, A.; Villiers, C. L.; Calemczuk, R.; Leroy, V.; Marche, P. N.; Livache, T.; Villiers, M.-B. *Clin. Chem.* **2006**, *52*, 255–262.
(2) Lofgren, J. A.; Dhandapani, S.; Pennucci, J. J.; Abbott, C. M.; Mytych, D. T.; Kaliyaperumal, A.; Swanson, S. J.; Mullenix, M. C. *J. Immunol.* **2007**, *178*, 7467–7472.
(3) Soelberg, S. D.; Chinowsky, T.; Geiss, G.; Spinelli, C. B.; Stevens, R.; Near, S.; Kauffman, P.; Yee, S.; Furlong, C. E. *J. Ind. Microbiol. Biotechnol.* **2005**, *32*, 669–674.
(4) Mauriz, E.; Calle, A.; Manclus, J. J.; Montoya, A.; Lechuga, L. M. *Anal. Bioanal. Chem.* **2007**, *387*, 1449–1458.
(5) Patel, P. D. *J. AOAC Int.* **2006**, *89*, 805–818.
(6) Nugen, S. R.; Baeumner, A. J. *Anal. Bioanal. Chem.* **2008**, *391*, 451–454.
(7) Homola, J. *Chem. Rev.* **2008**, *108*, 462–493.
(8) Kretschmann, E.; Raether, H. *Z. Naturforsch.* **1968**, *23a*, 2135–2136.
(9) Malyarchuk, V.; Hua, F.; Mack, N.; Velasquez, V.; White, J.; Nuzzo, R.; Rogers, J. *Opt. Express* **2005**, *13*, 5669–5675.
(10) Singh, B. K.; Hillier, A. C. *Anal. Chem.* **2006**, *78*, 2009–2018.
(11) Yao, J.; Stewart, M. E.; Maria, J.; Lee, T.-W.; Gray, S. K.; Rogers, J. A.; Nuzzo, R. G. *Angew. Chem., Int. Ed.* **2008**, *47*, 5013–5017.
(12) Eftekhari, F.; Escobedo, C.; Ferreira, J.; Duan, X.; Girrotto, E. M.; Brolo, A. G.; Gordon, R.; Sinton, D. *Anal. Chem.* **2009**, *81*, 4308–4311.
(13) Maynard, J. A.; Lindquist, N. C.; Sutherland, J. N.; Lesuffleur, A.; Warrington, A. E.; Rodriguez, M.; Oh, S.-H. *Biotechnol. J.* **2009**, *4*, 1542–1558.
(14) Yang, J.-C.; Ji, J.; Hogle, J. M.; Larson, D. N. *Nano Lett.* **2008**, *8*, 2718–2724.
(15) Lindquist, N. C.; Lesuffleur, A.; Im, H.; Oh, S.-H. *Lab Chip* **2009**, *9*, 382–387.
(16) Piliarik, M.; Homola, J. *Opt. Express* **2009**, *19*, 16505–16517.
(17) Yoon, K. H.; Shuler, M. L.; Kim, S. J. *Opt. Express* **2006**, *14*, 4842–4849.
(18) Kabashin, A. V.; Evans, P.; Pastkovsky, S.; Hendren, W.; Wurtz, A. G.; Atkinson, R.; Pollard, R.; Podolskiy, V. A.; Zayats, A. V. *Nat. Mater.* **2009**, *8*, 867–871.
(19) Lesuffleur, Antoine; Im, Hyungsoon; Lindquist, Nathan C.; Oh, S.-H. *Appl. Phys. Lett.* **2007**, *90*, 243110.
(20) Lee, K.-L.; Lee, C.-W.; Wang, W.-S.; Wei, P.-K. *J. Biomed. Opt.* **2007**, *12*, 04402.
(21) Henzie, J.; Lee, M. H.; Odom, T. W. *Nat. Nanotechnol.* **2007**, *2*, 549–554.
(22) Odom, T. W. *MRS Bull.* **2010**, *35*, 66–73.

DOI: 10.1021/nl101165r | *Nano Lett.* **2010,** *10,* 2549–2554

(23) Odom, T. W.; Thalladi, V. R.; Love, J. C.; Whitesides, G. M. *J. Am. Chem. Soc.* **2002**, *124*, 12112–12113.
(24) Gao, H.; Henzie, J.; Lee, M. H.; Odom, T. W. *Proc. Natl. Acad. Sci. U.S.A.* **2008**, *105*, 20146–20151.
(25) Gao, H.; Zhou, W.; Odom, T. W. *Adv. Funct. Mater.* **2009**, *19*, 529–539.
(26) Pei, R.; Cui, X.; Yang, X.; Wan, E. *Biomacromolecules* **2001**, *2*, 463–468.
(27) Raether, H., *Surface Plasmons on Smooth and Rough Surfaces and on Gratings*; Springer: Berlin and New York, 1988.
(28) Johnson, P. B.; Christy, R. W. *Phys. Rev. B* **1972**, *6*, 4370–4379.
(29) Hornauer, D.; Raether, H. *Opt. Commun.* **1973**, *7*, 297–301.
(30) Bozhevolnyi, S. I. *Opt. Express* **2006**, *14*, 9467–9476.
(31) Milton, J. D.; Fernig, D. G.; Rhodes, J. M. *Glycoconjugate J.* **2001**, *18*, 565–569.
(32) Houseman, B. T.; Gawalt, E. S.; Mrksich, M. *Langmuir* **2003**, *19*, 1522–1531.
(33) Su, J.; Mrksich, M. *Langmuir* **2003**, *19*, 4867–4870.
(34) Mrksich, M. *ACS Nano* **2008**, *2*, 7–18.
(35) Masel, R. I. *Principles of Adsorption and Reaction on Solid Surfaces.*, 1st ed.; Wiley-Interscience: New York, 1996; p 240.

DOI: 10.1021/nl101165r | *Nano Lett.* **2010,** *10,* 2549--2554